Geometrical model for martensitic phase transitions: Understanding criticality and weak universality during microstructure growth

Genís Torrents,[1] Xavier Illa,[2] Eduard Vives,[2] and Antoni Planes[2]
[1]*Departament de Física Quàntica i Astrofísica, Facultat de Física, Universitat de Barcelona, Martí i Franquès 1, E-08028 Barcelona, Catalonia*
[2]*Departament de Física de la Matèria Condensada, Facultat de Física, Universitat de Barcelona, Martí i Franquès 1, E-08028 Barcelona, Catalonia*
(Received 9 August 2016; published 3 January 2017)

A simple model for the growth of elongated domains (needle-like) during a martensitic phase transition is presented. The model is purely geometric and the only interactions are due to the sequentiality of the kinetic problem and to the excluded volume, since domains cannot retransform back to the original phase. Despite this very simple interaction, numerical simulations show that the final observed microstructure can be described as being a consequence of dipolar-like interactions. The model is analytically solved in 2D for the case in which two symmetry related domains can grow in the horizontal and vertical directions. It is remarkable that the solution is analytic both for a finite system of size $L \times L$ and in the thermodynamic limit $L \to \infty$, where the elongated domains become lines. Results prove the existence of criticality, i.e., that the domain sizes observed in the final microstructure show a power-law distribution characterized by a critical exponent. The exponent, nevertheless, depends on the relative probabilities of the different equivalent variants. The results provide a plausible explanation of the weak universality of the critical exponents measured during martensitic transformations in metallic alloys. Experimental exponents show a monotonous dependence with the number of equivalent variants that grow during the transition.

DOI: 10.1103/PhysRevE.95.013001

I. INTRODUCTION

Martensitic transformations are first-order solid-solid phase transitions in which the system undergoes a change in the symmetry of the crystalline lattice [1]. The high-symmetry phase, called austenite, is the stable phase at high temperatures. When cooling, the atoms rearrange without long-range diffusion into a less symmetric phase called martensite. In general, a group-subroup relationship exists between the symmetries of the austenite and martensite, which implies that the new martensitic domains can grow in different equivalent variants that are symmetrically related. The arrangement of the martensitic domains constitutes the so-called martensite microstructure [2] and is, to a large extent, determined by the minimization of the elastic strain field that results from the crystal misfit between the martensite and the parent phases [3,4].

In the absence of externally applied fields and in contrast to the prototypical first-order phase transitions, martensitic transformations do not usually occur at a well-defined temperature, but extend along a certain temperature range. The main reason for this extended behavior is due to the internal elastic forces (thermoelasticity) [5]. When a first domain nucleates in the bulk of an austenitic single crystal, it creates an internal stress field that arrests the transition, in a way similar to the pressure decrease one observes in vapor-liquid condensation at constant volume. Undercooling is needed for the transition to proceed. Other reasons behind the extended character are the existence of favorable nucleation centers on the crystal surfaces and/or the existence of impurities, vacancies, dislocations, etc. Stress fields around quenched disorder also contribute to the extended behavior by creating a range of effective local transition temperatures.

As a consequence of these combined effects, the final microstructure when the transition is complete (at low temperatures) may become quite complex, difficult to predict but with very important consequences for the macroscopic properties of the material. Microstructures can be easily observed by optical microscopy using polarized light, revealing the tiny deformations on the sample surface corresponding to the different variants. Figure 1 shows, as an example, a micrograph of a Cu-Zn-Al sample in the martensitic phase. The microstructure consists of an apparently random combination of thin martensite needles, as shown by the different colors corresponding to different symmetry-related variants. Fourier analysis of such microstructures indicates that the distribution of domain sizes tends to be fat-tailed in the large-size region [6,7].

It is more difficult to obtain experimental information about the growth dynamics, given the fast character of the martensite-austenite interface movements. Several martensitic transformations have been studied by using techniques with high-time resolution. Both acoustic emission [8,9] and high-sensitivity calorimetry [10] have revealed an intermittent behavior called avalanche dynamics: when cooling rate is slow enough, the system remains trapped in metastable states until a free-energy barrier disappears. Then, it relaxes, by creating a new martensite domain, in a fast event called an avalanche. After it, the system remains again in a silent period. In other words, within the time resolution reached by AE techniques (microseconds), the transformation process occurs as a sequence of transformation events with well-defined waiting times between them [11].

The study of the statistical properties of these avalanches has revealed that they tend to show absence of characteristic scales in energies, durations, sizes, etc. This is also revealed by the fat tails of the experimental distributions that, in many cases, fit very well to power laws with characteristic exponents. For the energy distributions, for instance, $p(E) \sim E^{-\epsilon}$. The relation between the absence of characteristic scales and the

FIG. 1. Example of the final microstructure on a $Cu_{69.3}Zn_{17}Al_{13.7}$ single crystal, after the thermally induced transformation from cubic to monoclinic phase is completed. The image corresponds to a $\sim$8 mm $\times$ 6 mm area approximately perpendicular to the the [100] direction. It has been obtained by using polarized light on a sample initially polished in the cubic phase. Different colors indicate slightly different orientations of the sample surface and, therefore, approximately correspond to different variants.

existence of an out-of-equilibrium critical point has been discussed [9]. This suggests that the exponents tend to show universal behavior. The universality, nevertheless, is weak. Analysis of different alloys that transform into different symmetries indicates that the exponent ϵ depends on the number of equivalent variants that grow during the transition. It takes values $\epsilon = 2, 1.75$, and 1.6 when the number of equivalent variants is 12, 6, and 4, respectively [9,12]

Microstructure modeling is based, essentially, in the calculation of combinations of variants minimizing elastic energy in the martensitic phase [13–15]. Models describe very well the existence of twins, which consists in two equivalent variants that grow one adjacent to the other forming a very elongated martensite needle that in some cases extend along the whole sample. Other more sophisticated solutions correspond to zigzag twins, twins within twins and many other complex variant organizations near defects. But most of these models neglect the fact that the microstructure should be grown dynamically during the cooling process and that, once a domain has grown into a certain variant, retransformations to the parent austenitic phase or variant-variant transitions are usually impossible due to the existence of high-energy barriers. Thus, the problem of modeling the final microstructure cannot be treated as a problem of finding the energetically most favorable final state. Instead, it is important to identify the energetically most favorable sequence of transformations; in general, thermal fluctuations are very low and the system cannot explore, at every temperature, the whole configuration space.

In this paper we present a very simple probabilistic model that explores the dynamical constraints that occur when martensite variants (or twins) are grown sequentially during the martensitic transition. In general, we will refer to the transformed regions as domains, without specifying whether they are single variants of martensite or twins. We propose a continuum and a discrete 2D realization of this model that essentially assumes only two ingredients: the elongated nature (needle shape) of the growing domains and the absence of retransformation events, which implies that martensite needles cannot cross each other. The aim of this paper is to show that with only these two ingredients (also present in most of the realistic models including long-range elasticity) the model is able to predict some general results concerning the statistical distribution of sizes of the martensite domains in the final microstructures. It suggests that the fat-tail behavior experimentally observed in the distributions of acoustic emission and calorimetric avalanches could arise from this dynamical constraint, although it will become a true power-law distribution only in very special limits.

From a general viewpoint the model developed in the present work can be considered to belong to the class of geometrically constrained probabilistic models, such as the random sequential addition problem [16], the fragmentation and multifragmentation problems[17], the sequential partitioning problem [18], and the random space-filling problem [19]. It also has connections with the study of percolation and jamming of linear segments [20,21]. Our model is specifically formulated for systems undergoing a martensitic transition and is solved in both the continuum and discrete cases. It is expected to provide responses to recently reported experimental results concerning avalanche-like dynamics, which is characteristic of this class of transformations. In fact, other geometrically constrained models have been proposed in the past to deal with martensitic transitions. It is worth mentioning the model published by Rao *et al.* [22]. It was aimed at explaining the scale invariance that has been observed during the growth of acicular martensites. The model considers the competition between the front velocity and the nucleation rate of the martensite grains. Interestingly, in the limit of infinite growth velocity this model reduces to a specific realization of the model developed in the present paper. The solution of the model in this limit has been reported in Ref. [23]. Using the language of the present work, this solution focuses on the sequential distribution of untransformed regions. Actually, the same point of view has been adopted by Ball *et al.* [24], who have proposed a model aimed at understanding the same experimental results as those that have motivated the present paper. Actually, the most significant differences between Ball's model and the present one concerns the interpretation of the sequence of transformed and untransformed regions and a different recipe for the sequential ordering of segments. We will discuss these issues in the last section of the paper.

In Sec. II we define the details of the model and perform computer simulations with various symmetries. This allows us to understand some effective dipolar-like interactions between martensite domains that occur simply due to kinetic constraints.

In Sec. III we solve heuristically a continuum version of the simplest version of the model in which domains are infinitely thin, i.e., essentially 1D lines that grow in the horizontal and vertical directions on a 2D square. In this case, despite the fact that the transformation is never complete due to the 1D character of the transformed domains, we obtain an expression for the distribution of lengths in the limit when the number of grown domains is very large.

In Sec. IV we solve analytically the discrete version of the model in which variants have a certain width a and grow on a discrete lattice with size $L \times L$. In this case, the transition can be completed, and we obtain exact expression for the distribution of domain lengths for any finite size L. Some interesting graphical examples are presented.

Finally, in Sec. VI we discuss and summarize the conclusions.

II. MODEL

The model under construction is defined on planar lattices with lattice spacing a. On the lattice we propose a set of equivalent directions that will correspond to the possible growth directions of the martensite needle domains. For instance, in the simplest case we consider only two equivalent domains growing in the horizontal $(1,0)$ and vertical $(0,1)$ direction, on a square lattice with $L \times L$ sites. We could also consider only two domains but growing along the diagonals $(1,1)$ and $(-1,1)$. This model would be equivalent to the first one except for the role played by the sample boundaries. Another example on the same square lattice will be to consider four growth directions along the directions $(1,2)$, $(2,1)$, $(-1,2)$, and $(-2,1)$. More complex symmetries can be defined on hexagonal lattices where we can select, for instance, three equivalent growth directions along $(1,0)$, $(0,1)$, and $(-1,1)$, etc.

Once the lattice and the equivalent directions have been defined, the microstructure is constructed as follows: (i) first, we choose a random site (uniformly distributed on the lattice) that has not been already transformed. (ii) Second, we sort according to a certain probability law, one of the equivalent directions. In the most common case, we use equal probabilities for every equivalent direction, but for the analytical analysis below we will also consider situations in which some directions are favored. In practice this could occur when the system is subjected to external fields that break the symmetry. (iii) Then, starting from the chosen site, a martensite domain is grown with width a (equal to one lattice spacing) along the chosen direction (in both senses) until hitting the system boundaries or hitting an already transformed site. The variable of interest is the length ℓ of this domain. (iv) The process is repeated sequentially until the whole lattice has been transformed to the martensitic phase. For numerical simulation purposes, it is convenient to keep a table of the untransformed sites. Otherwise, the simulation becomes very slow at the late stages of the transformation.

Figure 2 shows an example of how the microstructure grows. Figure 3 shows an example of the final microstructure in a simulation of a $L \times L = 8192^2$ square lattice with two

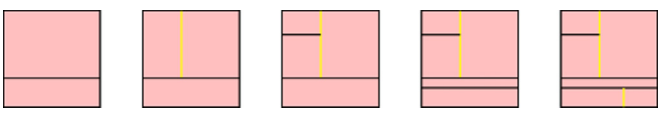

FIG. 2. Example of the initial domains in the construction of the microstructure with our model, in the case of two different equivalent domains along the (1,0) (black) and (0,1) (yellow) directions on a square lattice.

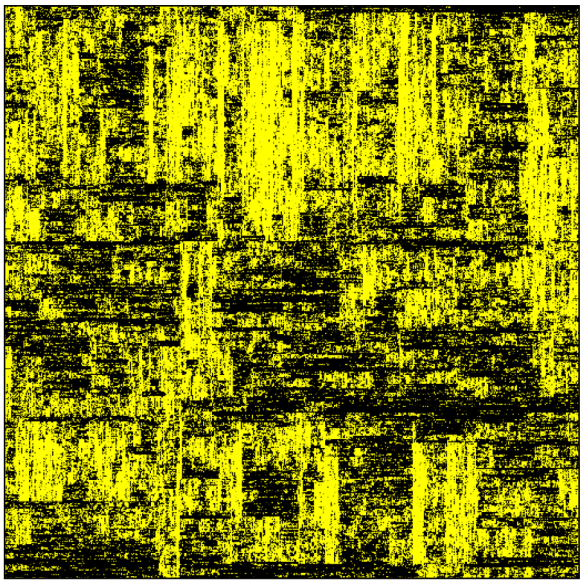

FIG. 3. Example of the final microstructure generated with our model, in the case of two different domains along the (1,0) (black) and (0,1) (yellow) directions on a square lattice. The lattice size for the simulation is $L = 8192$.

equally probable variants growing along the vertical and horizontal direction. The resolution of the plot does not allow to see the fine details of the microstructure. A magnified view is shown in Fig. 4. Details of the final microstructures corresponding to a case with three equivalent directions on a hexagonal lattice and four equivalent directions on a square lattice are shown in Figs. 5 and 6.

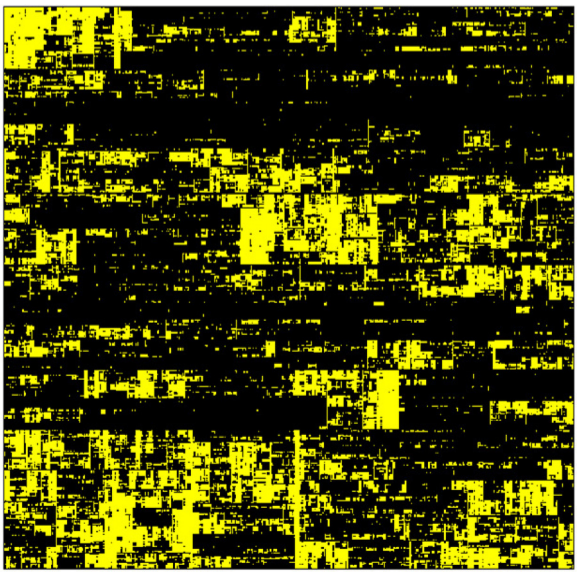

FIG. 4. Magnification of the final microstructure generated with our model, in the case of two different domains along the (1,0) (black) and (0,1) (yellow) directions on a square lattice. The original lattice size for the simulation is $L = 8192$. Only a small region of 500×500 sites is shown.

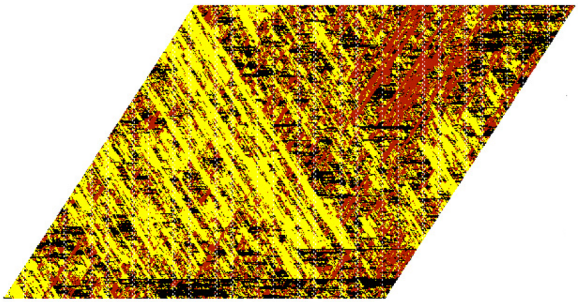

FIG. 5. Example of final microstructure generated with our model, in the case of three different domains along the (1,0) (black), (0,1) (red), and (−1,1) (yellow) directions on a hexagonal lattice, with equal probabilities. The simulated domain has a hexagonal shape with size $L = 8192$. Only an small area of 500×500 sites is shown.

The observation of the final microstructures reveals, at first sight, a surprising result: a clear tendency for domains that grow in the same direction (same color in the plots) to aggregate and form large regions. This correlation is also clear close to the system boundaries in Fig. 3. Horizontal (black) domains concentrate along the upper and lower boundaries, whereas vertical domains (yellow) concentrate along the right and left boundaries. Such correlations are very different from what one would expect after a random coloring problem. It is easy to understand that, effectively, there is indeed a dipolar-like interaction that favors both (i) martensite domains to grow in the same direction as boundaries nearby and (ii) domains growing in the same direction when they are close to one another.

Consider a certain empty region that, by chance, contains two parallel martensite domains in, for instance, the vertical direction (The same can be argued with a domain parallel to a boundary.) The empty sites in between these two domains have, *a priori*, the same probability for being filled with vertical or horizontal domains. But, if a horizontal domain grows in between these two vertical lines, it will have a very short length. Contrarily, if a vertical domain grows, it will have a much longer length and, thus, it will fill a bigger space. Therefore, *a posteriori*, the sites close to a certain domain are more probably filled by domains in the same direction.

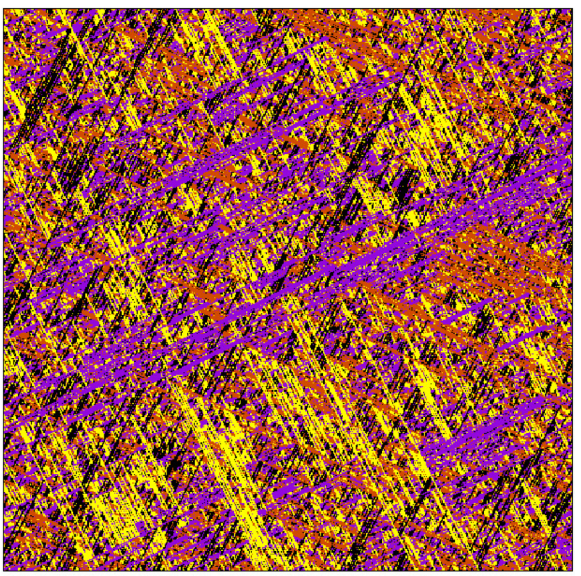

FIG. 6. Example of the final microstructure generated with our model, in the case of four different variants along the (1,2) (black), (2,1) (magenta), (−1,2) (yellow), and (−2,1) (red) directions on a square lattice, generated with equal probabilities. The lattice size is $L = 8192$. Only a small region of 500×500 sites is shown.

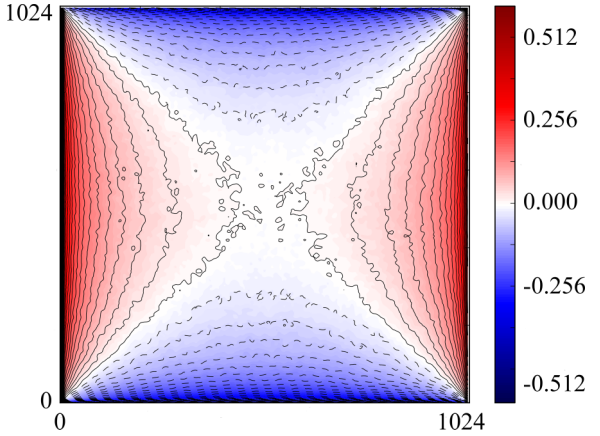

FIG. 7. Order parameter density indicating the relative probability of sites occupied by vertical or horizontal domains. Data corresponds to an average of many simulations of lattices with size $L = 8182$. The order parameter is measured on regions with size 8×8. When all 64 sites in the region are filled with vertical (horizontal) variants, the order parameter is 1 (−1).

One can thus conclude that, as a consequence of the dynamic constraints, martensitic domains show an effective dipolar-like attraction. By performing a large number of simulations we have evaluated the decay of such correlations with the distance. On the $L \times L = 8192^2$ lattice we have defined blocks of 8×8 sites and computed an order parameter that accounts for the difference in the coarse-grained density of vertical and horizontal domains. The result is shown in Fig. 7.

The plot reveals that the correlations with the boundaries are weak (order parameter changes below 2%) but long ranged, extending until reaching the center of the system. Such correlations can be measured in the surroundings of any domain.

In the following sections we will concentrate on the study of the distribution of domain lengths in the simplest case consisting in a square lattice with two equivalent variants growing in the horizontal and vertical direction.

III. CONTINUUM LIMIT

In order to study the variants of lengths ℓ much larger than the lattice spacing, i.e., in the limit $a/L \lesssim a/\ell \to 0$ one may consider a continuum version of the model in which all lengths are rescaled by L. Note that the results obtained by this rescaling may not work for those physical properties that are controlled by the finite width of the martensitic domains.

We consider a 2D square whose width and height have been rescaled to 1, and two directions for the martensite needles, namely (1,0) and (0,1) which are, now, 1D segments. Of course, in this continuum case, the system is never fully

transformed, but one may expect that after enough segments are drawn the statistical properties of the segments become stationary. We are interested in determining the distribution of domain lengths $z = \ell/L$ in such stationary regime. Note that z is a real number ($0 < z \leqslant 1$) in this continuum rescaled model. Due to the random nature of the process, the information about the distribution of lengths will be given by the average number density of domains with size in $(z, z + dz)$. For reasons that will become clear later, it is interesting to generalize the model allowing the two possible directions to be selected with different probabilities, p_h for horizontal domains and p_v for vertical domains. The focus of our attention will be the case $p_h + p_v = 1$, although our results in terms of p_h and p_v can be directly extrapolated to cases where $p_h + p_v < 1$, which might be suitable to address incomplete transitions in a hierarchy-less manner, i.e., with statistical (and dynamical) independence between regions of the lattice that have become isolated from each other during the process. The quantity of interest we will analyze is thus $H(z; p_h, p_v)$, the average number density of horizontal segments. The explicit dependence with the parameters p_h and p_v will be indicated only when needed.

In order to determine this quantity, in what follows, we will formulate an heuristic argument. First of all, take into account that the casuistics for $z = 1$ (that corresponds to the system length) are different from the rest of possible values. While there is a finite probability of generating a segment of $z = 1$ in our system as long as $p_h > 0$, any other specific size supposes, in the continuum limit, a set of zero measure in the domain of the distribution. Thus, it is reasonable to assume that

$$H(z; p_h, p_v) = A(p_h, p_v)\delta(z - 1) + h(z; p_h, p_v), \qquad (1)$$

where δ is Dirac's δ, $h(z; p_h, p_v)$ is a continuum function and does not vanish in the interval $(0,1)$ and A is a constant to be determined. On the other hand, given the continuum character of the problem, we can assume that the regions that are left after drawing the first segment are fully equivalent to the initial region but rescaled. Since we are interested in studying the length of horizontal segments we should care about rescaling only when the line that has been drawn is vertical. Considering this first drawing, the problem can thus be split as

$$H(z; p_h, p_v) = p_h H^{[h]}(z) + p_v H^{[v]}(z), \qquad (2)$$

where $H^{[h]}(z)$ [$H^{[v]}(z)$] is the average number density if the first line is horizontal (vertical). Let us consider the two cases separately. If the first line is horizontal the two new areas are exactly as the original one without rescaling. Therefore, from Eq. (1) we can write

$$H^{[h]}(z) = 1\delta(z - 1) + 2[A\delta(z - 1) + h(z)], \qquad (3)$$

where the first term corresponds to the horizontal line that has been drawn and the second term to the two equivalent problems above and below the line.

If the first line is vertical, one should rescale the new two problems according to the position x where the first line was drawn. The problem on the right will be rescaled by a factor $(1 - x)$ and the problem on the left by a factor x. For symmetry reasons it is enough to study the problem on the left and multiply the result by a factor of 2. The variable x is, *a priori*, uniformly distributed between 0 and 1. But if x turns out to be smaller than z, $H^{[v]}(z)$ in the left region becomes zero because no more segments of size z can exist. Thus, we can write

$$H^{[v]}(z) = 2\int_0^1 dx\Theta(x - z)\left[\frac{A}{x}\delta\left(\frac{z}{x} - 1\right) + \frac{1}{x}h\left(\frac{z}{x}\right)\right], \qquad (4)$$

where Θ is a heaviside function that takes into account the above-mentioned limitation for $x > z$. Performing a change of variables ($t = z/x, dt = -zdx/x^2$) and joining the above expressions (1)–(3), and (4) one gets the following integral equation:

$$A\delta(z - 1) + h(z) = p_h[(1 + 2A)\delta(z - 1) + 2h(z)] + p_v\left[2A + 2\int_z^1 h(t)\frac{dt}{t}\right]. \qquad (5)$$

This equation can be easily solved. Analyzing the term that multiplies the δ function one gets

$$A = \frac{p_h}{1 - 2p_h}. \qquad (6)$$

In turn, the equation obtained for the continuum part of the distribution is

$$h(z)(1 - 2p_h) = \frac{2p_h p_v}{1 - 2p_h} + 2p_v\int_z^1 h(t)\frac{dt}{t}. \qquad (7)$$

After differentiating with respect to z the following linear differential equation is obtained:

$$\frac{dh}{dz} = -\frac{2p_v}{1 - 2p_h}\frac{h}{z}. \qquad (8)$$

The solution is a power-law function: $h(z) \propto z^{-2p_v/(1-2p_h)}$. By adjusting the proportionality constant, one finally obtains

$$H(z) = \frac{p_h}{1 - 2p_h}\delta(z - 1) + \frac{2p_h p_v}{(1 - 2p_h)^2}z^{-\frac{2p_v}{1-2p_h}}. \qquad (9)$$

Thus, besides the δ contribution at $z = 1$, the average distribution density of lengths $H(z)$ will be a power law $z^{-\alpha}$ with an exponent α that depends on p_h and p_v. A particularly interesting case occurs when $p_h \to 0$. Almost all the segments are vertical and the few horizontal lines are distributed as z^{-2}. Nevertheless, notice that the exponent diverges for $p_h = 1/2$ (which is the symmetric and, perhaps, most interesting case) and it gives a nonsensible positive value for larger values of p_h. The origin of these unphysical results is the absence of a limiting mechanism in our argument for the number of lines of $z = 1$. When $p_h \ll 1/2$ this role is played by statistics itself and the problem disappears. In any physical construction, at $p_h \sim 1/2$ a small size effect (the UV cutoff of the problem), such as the line size or the lattice spacing, would supersede statistics in this duty. Note than under the standard assumption that $p_h + p_v = 1$, the exponent becomes $\alpha(p_h) = (2 - 2p_h)/(1 - 2p_h)$. But, if $p_h + p_v = c < 1$, we will have an smaller exponent $\alpha(p_h) = (2c - 2p_h)/(1 - 2p_h)$.

IV. EXACT SOLUTION

Let us now derive the exact solution for the discrete case. We consider a finite lattice with $L \times L$ sites and a lattice spacing a. Domains are elongated and have a width a and a variable

length ℓ. The variable ℓ now takes discrete values between 1 and L.

For the computation below, it is important to introduce the dependence with the system size and allow the horizonal and vertical lengths to be different. The function $H_{\ell;L_h,L_v}(p_h,p_v)$ will now describe, not the average density, but the average number of horizontal variants with length ℓ. To proceed, we develop a recurrence relation for $H(\ell)$. For this purpose, let us study what happens when the first line is drawn. Following an analogous treatment to the one in the previous section we get

$$H_{\ell;L_h,L_v} = p_h\delta_{\ell L_h} + \frac{2p_h}{L_v}\sum_{j=1}^{L_v-1} H_{\ell;L_h,j} + \frac{2p_v}{L_h}\sum_{j=\ell}^{L_h-1} H_{\ell;j,L_v}. \tag{10}$$

It is straightforward to check that this recurrence can be simplified to

$$\begin{aligned} H_{\ell;L_h,L_v} &- \frac{L_v-1+2p_h}{L_v}H_{\ell;L_h,L_v-1} - \frac{L_h-1+2p_v}{L_h}H_{\ell;L_h-1,L_v} \\ &+ \frac{(L_v-1+2p_h)(L_h-1+2p_v)-4p_hp_v}{L_vL_h}H_{\ell;L_h-1,L_v-1} \\ &= \frac{p_h}{L_v}\left(\delta_{\ell,L_h} - \frac{L_h-1}{L_h}\delta_{\ell,L_h-1}\right). \end{aligned} \tag{11}$$

Note that the solution of the homogeneous part of this linear recurrence, i.e., the set of values H_{ℓ,L_h,L_v} for which the left-hand side of Eq. (11) vanishes, includes the constructions $A^{L_h,L_v}_{k,\ell_h,\ell_v}(2p_v,2p_h)$, defined by the following rule:

$$A^{L_h,L_v}_{k,\ell_h,\ell_v}(x_h,x_v) \equiv \sum_{j=0}^{\infty}\frac{x_h^j x_v^{j+k}}{j!(j+k)!}\frac{d^{2j+k}\Delta^{L_h,L_v}_{\ell_h,\ell_v}}{dx_h^j dx_v^{j+k}}, \tag{12}$$

with

$$\Delta^{L_h,L_v}_{\ell_h,\ell_v}(x_h,x_v) \equiv \frac{\ell_h!\Gamma(x_h+L_h)}{L_h!\Gamma(x_h+\ell_h)}\frac{\ell_v!\Gamma(x_v+L_v)}{L_v!\Gamma(x_v+\ell_v)}. \tag{13}$$

In Eq. (12) it must be understood that k is an integer and that, when it is negative, only terms with positive or zero factorials in the divisor will contribute. It is worth pointing out that Δ is a polynomial of finite degree and consequently so are the functions A; their expression as an infinite sum is merely convenient for the purposes of this paper, and in general more compact expressions for these quantities might be more appropriate, such as

$$A^{L_h,L_v}_{k,\ell_h,\ell_v}(x_h,x_v) = \frac{\oint z^{k-1}\Delta^{L_h,L_v}_{\ell_h,\ell_v}(x_h+x_hz,x_v+x_v/z)dz}{2\pi i}. \tag{14}$$

Before we proceed, let us point out two properties of these objects that will be relevant later on:

(1) Symmetry:

$$A^{L_h,L_v}_{k,\ell_h,\ell_v}(x_h,x_v) = A^{L_v,L_h}_{-k,\ell_v,\ell_h}(x_h,x_v). \tag{15}$$

(2) Sum completion:

$$\sum_{k=-\infty}^{\infty} a^k A^{L_h,L_v}_{k,\ell_h,\ell_v}(x_h,x_v) = \Delta^{L_h,L_v}_{\ell_h,\ell_v}\left(x_h+\frac{x_h}{a},x_v+ax_v\right). \tag{16}$$

In order to solve Eq. (11) completely, it will suffice to build a linear combination of $A^{L_h,L_v}_{k,\ell_h,\ell_v}(2p_v,2p_h)$ of different k, ℓ_h, and ℓ_v that vanishes whenever $L_v=0$, and matches the appropriate boundary conditions at $\ell = L_h-1$. Unless otherwise stated, it will be understood in the rest of the paper that the arguments of $A^{L_h,L_v}_{k,\ell_h,\ell_v}$ functions are $x_h = 2p_v$ and $x_v = 2p_h$, respectively.

Let us now explain how these boundary conditions can be established. We begin observing that when $L_v = 1$ the only way to have a horizontal line of size $\ell = L_h$ is for it to be the first drawn line:

$$H_{L_h;L_h,1} = p_h. \tag{17}$$

Consequently, from Eq. (11), we get directly

$$H_{L_h-1;L_h,1} = \frac{2p_vp_h}{L_h}. \tag{18}$$

Then, we extend this result to generic L_v by using the recurrence Eq. (11), which, in the case $\ell = L_h$, can be rewritten in a suggestive way:

$$\begin{aligned} H_{L_h;L_h,L_v} &- \frac{p_h}{1-2p_h} \\ &= \frac{2p_h+L_v-1}{L_v}\left(H_{L_h;L_h,L_v-1} - \frac{p_h}{1-2p_h}\right). \end{aligned} \tag{19}$$

From this result it follows that

$$H_{L_h;L_h,L_v} = \frac{p_h}{1-2p_h}\left[1 - \frac{2p_h}{L_v!}\frac{\Gamma(2p_h+L_v)}{\Gamma(2p_h+1)}\right]. \tag{20}$$

Observe that the first term inside the parenthesis corresponds to the continuum limit prediction, the prefactor of δ in Eq. (9). We obtain $H_{L_h-1;L_h,L_v}$ in a similar way, making use of the recurrence Eq. (11), which, after the substitution of Eq. (20), reads

$$H_{L_h-1;L_h,L_v} = \frac{2p_h+L_v-1}{L_v}H_{L_h-1;L_h,L_v-1} + \frac{2p_hp_v}{L_vL_h(1-2p_h)}\left[1 - \frac{(2p_h)^2\Gamma(2p_h+L_v-1)}{(L_v-1)!\Gamma(2p_h+1)}\right]. \tag{21}$$

We thus apply this recurrence on Eq. (18) and generate

$$H_{L_h-1;L_h,L_v} = \frac{2p_hp_v}{L_h(1-2p_h)^2}\left\{1 + \frac{\Gamma(2p_h+L_v)}{L_v!\Gamma(2p_h+1)}2p_h\left[(2-2p_h) + (1-2p_h)\sum_{k=1}^{L_v-1}\frac{1}{k+2p_h}\right]\right\}. \tag{22}$$

This equation in conjunction with the aforementioned restriction, $H_{\ell,L_h,0}=0$, constitutes the boundary conditions for the remaining problem.

We are now in a position to build the general solution for the recurrence as a linear combination of the quantities $A^{L_h,L_v}_{k,\ell_h,\ell_v}$, which we introduced in Eq. (12). From the minutious analysis of Eq. (22) we obtain the main result of this section:

$$H_{\ell<L_h;L_h,L_v}=\frac{2p_hp_v}{(1-2p_h)^2(\ell+1)}\left\{\sum_{j=0}^{\infty}\left(\frac{1}{2p_h}-1\right)^j A^{L_h,L_v}_{j;\ell+1,1}-2p_h\left[(2-2p_h)A^{L_h,L_v}_{0;\ell+1,1}+(1-2p_h)A^{L_h,L_v}_{1;\ell+1,1}\right]\right\}. \tag{23}$$

The key point in this last step is to observe that at $\ell=L_h-1$ the defining sum for the quantities $A^{L_h,L_v}_{k,\ell+1,\ell_v}$ in Eq. (12) has a single nonvanishing term: $j=0$.

Let us analyze some specific limits of interest of this expression before closing this section:

Regime $p_h\ll 1/2$: It is convenient to use the sum completion property Eq. (16) in order to make explicit the divergence cancellation in the first parenthesis of Eq. (23). Thereafter,

$$H_{\ell;L_h,L_v}=\frac{2p_hp_v\left[\Delta^{L_h,L_v}_{\ell,1}\left(\frac{2p_v}{1-2p_h},1\right)+\mathcal{O}(p_h)\right]}{(1-2p_h)^2(\ell+1)}. \tag{24}$$

Using the Stirling approximation one recovers the continuum distribution in Eq. (9), up to an L_h^{-1} factor that disappears when we rephrase the distribution in terms of $z=\ell/L_h$,

$$H_{\ell;L_h,L_v}\sim\frac{2p_hp_v}{(1-2p_h)^2L_h}\left(\frac{\ell_h}{L_h}\right)^{-\frac{2p_v}{1-2p_h}}. \tag{25}$$

The corrections to this result at finite p_h are controlled by $4p_vp_h/(1-2p_h)$, so the continuum solution should be mistrusted at $p_h\gtrsim 0.19$ (provided $p_h+p_v=1$).

Regime $p_h\sim 1/2$: Let us rewrite Eq. (23) as

$$H_{\ell;L_h,L_v}=\frac{2p_hp_v}{(\ell+1)}\left[A^{L_h,L_v}_{0;\ell+1,1}+\frac{1+2p_h}{2p_h}A^{L_h,L_v}_{1;\ell+1,1}+\frac{1}{4p_h^2}\sum_{j=0}^{\infty}\left(\frac{1-2p_h}{2p_h}\right)^j A^{L_h,L_v}_{j+2;\ell+1,1}\right]. \tag{26}$$

This expression is manifestly finite and well behaved at $2p_h\to 1$. Similarly, the result of Eq. (20) for $\ell=L_h$ becomes in this limit

$$H_{L_h,L_h,L_v}=\frac{1}{2}(\psi(L_h+1)+\gamma_E)\sim\frac{\log L_h+\gamma_E}{2}, \tag{27}$$

where ϕ is the digamma function, and γ_E denotes the Euler-Mascheroni constant. Observe the qualitative difference between these results and those in the regime of $p_h\ll 1/2$. The absence of the power-law behavior and the dependence of H_{L_h,L_h,L_v} on the size are both consequence of the active role of the cutoffs of the problem in the regularization of the amount of horizontal lines crossing the system.

Regime $p_h=1-p_v\to 1$. In this limit the A functions will be dominated by the first term of their defining series, and therefore, the first parenthesis of Eq. (16) becomes a formal Taylor series in x_v in the explicit limit. Making use again of Stirling's approximation we obtain for the continuum part of the distribution

$$H_{\ell;L_h,L_v}\sim\frac{2p_v}{L_h}\sqrt{\frac{L_v}{\ell_v}}(1+2H_{1+L_v}-2H_2)+\mathcal{O}(p_v^2), \tag{28}$$

where H_n denotes the nth harmonic number. Notice that the leading contribution in this limit is generated from the case where a single vertical line is generated, and since any position for this variant is equiprobable the ℓ dependence disappears.

V. NUMERICAL COMPUTATION

At large L and ℓ, it becomes an imperative to identify better strategies to evaluate $A^{L_h,L_v}_{k;\ell_h,\ell_v}$ than their defining sum: the direct implementation of the latter wastes more computational resources than the full recurrence Eq. (11). In this section we will present an algorithm to evaluate this quantity in a more efficient way for our purposes.

The key point in what follows is that in $A^{L_h,L_v}_{k;\ell_h,\ell_v}$ the L and ℓ variables mirror each other. It is straightforward to verify that a similar recurrence to the homogeneous part of Eq. (11) holds, where the roles of ℓ and L variables are interchanged:

$$A^{L_h,L_v}_{k;\ell_h,\ell_v}=\frac{(2p_v+\ell_h)}{\ell_h+1}A^{L_h,L_v}_{k;\ell_h+1,\ell_v}+\frac{(2p_h+\ell_v)}{\ell_v+1}A^{L_h,L_v}_{k;\ell_h,\ell_v+1}+\frac{2p_h2p_v-(2p_v+\ell_h)(2p_h+\ell_v)}{(\ell_h+1)(\ell_v+1)}A^{L_h,L_v}_{k;\ell_h+1,\ell_v+1}. \tag{29}$$

Admittedly, the evaluation of a single value in a specific A construction is not necessarily simpler in Eq. (29) than in the homogeneous part of Eq. (11). The main advantage of using Eq. (29) is the fact that, in contrast to what happens for Eq. (11), we do not have to obtain the A values at any L_v and L_h independently for a specific ℓ. Instead, we obtain all the $\ell<L_h$ part of the distribution at a time for a specific L_v and L_h.

Therefore, we determine the value of Eq. (23) by applying the recurrence Eq. (29) on its combination of A_k structures, which we will denote by $\tilde{A}$, and which satisfy the boundary conditions

$$\tilde{A}^{L_h,L_v}_{L_h,\ell_v}=\frac{2p_hp_v}{(1-2p_h)^2}\left\{1-2p_h\frac{\ell_v!\Gamma(L_v+2p_h)}{L_v!\Gamma(\ell_v+2p_h)}\left[(2-2p_h)+2p_h(1-2p_h)\left(H_{L_v+2p_h-1}-H_{\ell_v+2p_h-1}\right)\right]\right\},$$
$$\tilde{A}^{L_h,L_v}_{\ell_h,L_v}=\frac{2p_hp_v\ell_h!\Gamma(L_h+2p_v)}{L_h!\Gamma(\ell_h+2p_v)}. \tag{30}$$

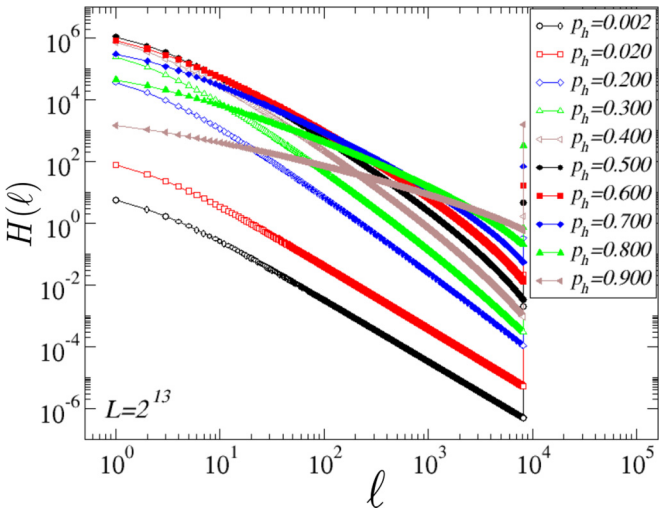

FIG. 8. Average number of domains with length ℓ for a system with size $L = 2^{13}$ and different values of p_h, as indicated in the legend. Lines are guides to the eye.

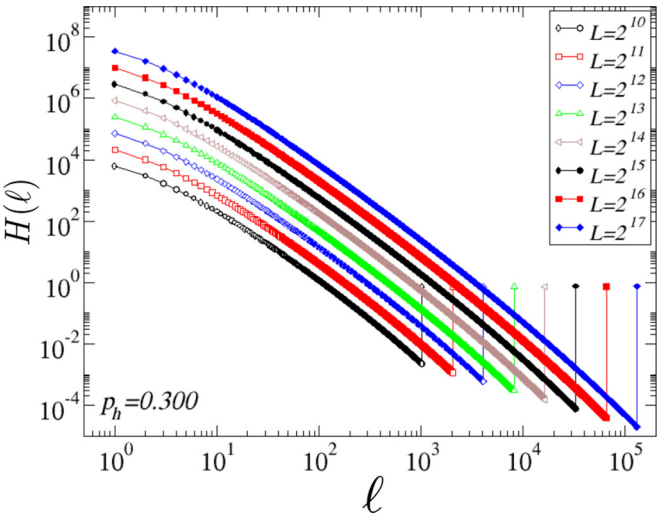

FIG. 10. Average number of domains with length ℓ for $p_h = 0.3$, and different system sizes as indicated in the legend. Lines are guides to the eye.

We can directly read $H_{\ell,L_h,L_v} = (1-\ell)^{-1}\tilde{A}^{L_h,L_v}_{\ell+1,1}$ as long as $\ell < L_h$. The distribution is completed with the H_{L_h,L_h,L_v} value given by Eq. (20).

In the following pictures we graphically illustrate the behavior of the distribution of avalanche sizes for different values of p_h ($p_v = 1 - p_h$) and L. Figure 8 shows, in a log-log plot, the average number of domains with length ℓ for a fixed system size $L \times L = 8192^2$ and several values of p_h increasing from 0.02 to 0.9. As can be seen up to $p \simeq 0.4$ the tail exhibits a reasonable power-law (linear) behavior. The distributions show a δ-function-like behavior for $\ell = L = 8192$, which corresponds to the values given by Eq. (20).

Figure 9 shows the same distributions as in Fig. 8 but for a larger system size $L = 2^{17} = 131\,072$. One can observe that the power-law tails for small values of p extend now to more than four decades, between $\ell = 10$ and $\ell = 10^5$. For large values of p the curvatures do not disappear.

The same conclusion can be reached by plotting the same distributions for a fixed value of p_h and for increasing values of L, as shown in Figs. 10 and 11.

It is worth noticing that the height of the δ-function-like peak at $\ell = L$ shows an constant behavior for $p_h = 0.3$, but shows an increasing logarithmic behavior for $p_h = 0.5$, as discussed in the paragraph after Eq. (27).

For the values of p_h smaller than 0.5 it is possible to define an effective exponent corresponding to the power-law-like behavior $H(\ell) \sim \ell^{-\alpha}$ of the tail of the observed distributions. We have chosen to fit it by estimating the logarithmic derivative

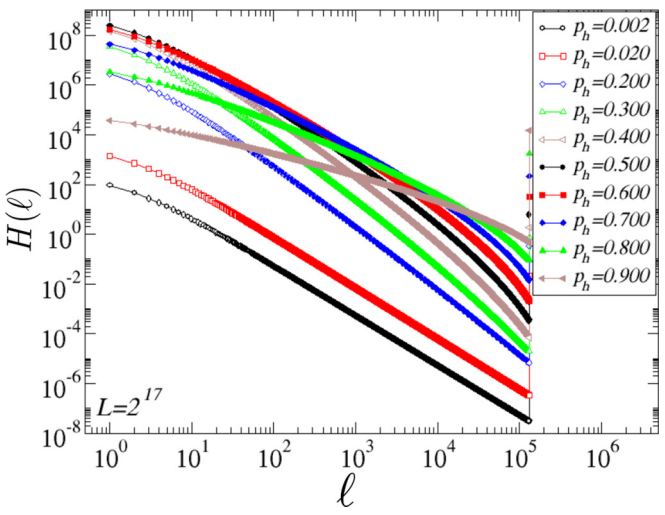

FIG. 9. Average number of domains with length ℓ for a system with size $L = 2^{17}$ and different values of p_h, as indicated in the legend. Lines are guides to the eye.

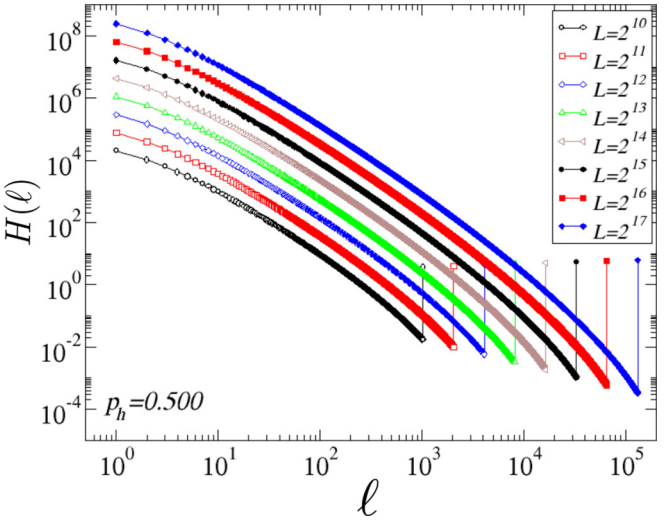

FIG. 11. Average number of domains with length ℓ for $p_h = 0.5$, and different system sizes as indicated in the legend. Lines are guides to the eye.

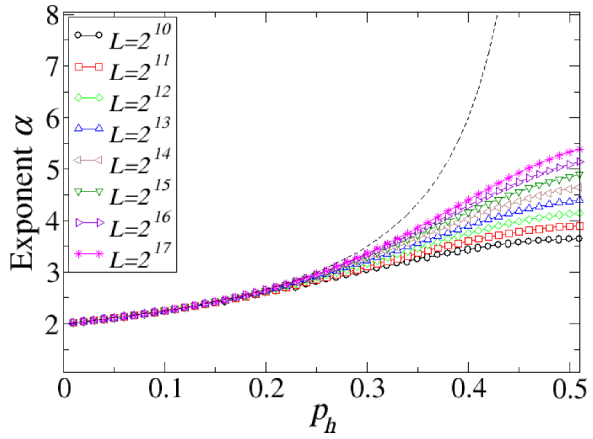

FIG. 12. Exponent fitted at the central part of the distribution as a function of the probability of horizontal variants p_h for different system sizes L as indicated in the legend. The black dashed line shows the behavior corresponding to the continuum limit, given in Eq. (9).

at $\ell = L - 1$ (avoiding the δ-function-like peak at $\ell = L$) as

$$\alpha = -\left.\frac{d\log H}{d\log \ell}\right|_{\ell=L-1} \simeq (L-1)\left[\frac{H(L-2)}{H(L-1)} - 1\right]. \quad (31)$$

The results are shown in Fig. 12 as a function p_h. The dashed black line corresponds to the solution of the continuous model $\alpha = \frac{2(1-p_h)}{1-2p_h}$. The plot illustrate the slow convergence to the exact exponent in the limit $L \to \infty$ for $0.25 < p_h < 0.5$.

VI. DISCUSSION AND CONCLUSIONS

We have presented a simple geometrical model for the growth of needle-like domains in a 2D lattice, which can be easily applied to the study of 2D martensitic transitions by selecting the appropriate lattice symmetries and equivalent variants. Explicit analytic results for the model are presented for its simplest realization, which concerns only two variants. Its extension to 3D structural transitions would require us to consider planar domains growing in a 3D lattice. The formulation of such realizations of the model does not seem to be especially difficult, but the solution would in general be much more cumbersome.

In the Introduction we mentioned the close connection of this model with the one recently reported model by Ball *et al.* [24]. The authors consider the simplest continuum case on a 2D square and lines drawn at random and growing along the vertical or horizontal direction with a certain probability until hitting an exiting line or boundary. Every new line drawn separates the system into two rectangular domains. In contraposition to the approach presented here, in Ref. [24] the interest is centered on the distribution of untransformed regions. In addition, the model presented there differs with the present model in the fact that, in order to derive asymptotic expression for the number of rectangles with sizes (a,b) they choose the nucleation centers always in the domain with largest area, which induces an unphysical hierarchy in the problem and makes its statistical analysis considerably more involved.

It is worth pointing out that the two-variant implementation of our model features compelling properties: First, our analysis shows that certain quantities display criticality, which can be addressed analytically both in the large L limit and at finite size. This is a result that represents an important step in the understanding of the finite-size effects in critical systems. Second, our numerical experimentation indicates that the system has effective long-range interactions, but a critical behavior that depends on model parameters and that qualitatively differs from mean-field predictions. This is another surprising and interesting result. Third, another lesson uncovered by our treatment is the emergence of finite-size effects even at large L as $p_h \to 0.5$. This effect is unrelated to the equiprobability of variants. Instead, it comes from the role of the cutoffs of the problem in keeping finite the amount of horizontal needles expected for any subsystem. Consequently, the appearance of this effect will remain at $p = 0.5$ for the variant under consideration, even when the probability for the other variant is lowered, or when additional variants are included in the problem.

The present authors plan to study the local properties of the model, the already discussed extension to 3D, and to relax the condition for fixed width a, in the near future.

ACKNOWLEDGMENTS

We acknowledge financial support from the Spanish Ministry of Economy and Competitiveness (MAT2016-75823-R, MAT2015-69777-REDT). G.T. is partially supported by the same Ministry under Projects No. FPA2013-46570-C2-2-P and No. MDM-2014-0369 of ICCUB (Unidad de Excelencia María de Maeztu), and by AGAUR, Grant No. 2014-SGR-1474, and has been further supported by an FI scholarship (Generalitat de Catalunya). E.V. acknowledges the hospitality and scientific discussions with J. Ball, P. Cesana, and B. Hambly during a visit to the Oxford Mathematical Institute. We finally acknowledge M. Morin (INSA, Lyon) for giving us permission to publish the illustrative picture in Fig. 1.

[1] *Shape Memory Materials*, edited by K. Otsuka and C. M. Wayman (Cambridge University Press, Cambridge, 1998).

[2] K. Bhattacharya, *Microstructure of Martensite: Why It Forms and How It Gives Rise to the Shape Memory Effects* (Oxford University Press, Oxford, 2003).

[3] A. G. Kachaturyan, *Theory of Structural Transformations in Solids* (Dover, New York, 2008).

[4] M. Porta, T. Castán, P. Lloveras, T. Lookman, A. Saxena, and S. R. Shenoy, Phys. Rev. B **79**, 214117 (2009).

[5] O. U. Salman, A. Finel, R. Delville, and D. Schryvers, J. Appl. Phys. **111**, 103517 (2012).

[6] A. Yu. Pasko, A. A. Likhachev, Yu. N. Koval, and V. I. Kolomytsev, J. Phys. IV France **07**, C5-435 (1997).

[7] A. A. Likhachev, J. Pons, E. Cesari, A. Yu. Pasko, and V. I. Kolomytsev, Scr. Mater. **43**, 765 (2000).

[8] Ll. Carrillo, Ll. Mañosa, J. Ortín, A. Planes, and E. Vives, Phys. Rev. Lett. **81**, 1889 (1998).
[9] A. Planes, Ll. Mañosa, and E. Vives, J. Alloys Comp. **577**, S699 (2013).
[10] M. C. Gallardo, J. Manchado, F. J. Romero, J. del Cerro, E. K. H. Salje, A. Planes, E. Vives, R. Romero, and M. Stipcich, Phys. Rev. B **81**, 174102 (2010).
[11] J. Baró, J. M. Martín-Olalla, F. J. Romero, M. C. Gallardo, E. K. H. Salje, E. Vives, and A. Planes, J. Phys.: Condens. Matter **26**, 125401 (2014).
[12] E. Vives, J. Baró, M. C. Gallardo, J. M. Martín-Olalla, F. J. Romero, S. L. Driver, M. A. Carpenter, E. K. H. Salje, M. Stipcich, R. Romero, and A. Planes, Phys. Rev. B **94**, 024102 (2016).
[13] J. M. Ball and R. D. James, Arch. Ration. Mech. Anal. **100**, 13 (1987).
[14] L. Q. Chen, Annu. Rev. Mater. Res. **32**, 113 (2002).
[15] T. Lookman, S. R. Shenoy, K. O. Rasmussen, A. Saxena, and A. R. Bishop, Phys. Rev. B **67**, 024114 (2003).
[16] G. Tarjus and P. Viot, Phys. Rev. Lett. **67**, 1875 (1991).
[17] P. L. Krapivsky and E. Ben-Naim, Phys. Rev. E **50**, 3502 (1994).
[18] C. Frontera, J. Goicoechea, I. Ràfols, and E. Vives, Phys. Rev. E **52**, 5671 (1995).
[19] M. A. Etzold, P. J. McDonald, D. A. Faux, and A. F. Routh, Phys. Rev. E **92**, 042106 (2015).
[20] Lj. Budinski-Petkovic and U. Kozmidis-Luburic, Phys. Rev. E **56**, 6904 (1997).
[21] G. Kondrat and A. Pekalski, Phys. Rev. E **63**, 051108 (2001).
[22] M. Rao, S. Sengupta, and H. K. Sahu, Phys. Rev. Lett. **75**, 2164 (1995).
[23] E. Ben-Naim and P. L. Krapivsky, Phys. Rev. Lett. **76**, 3234 (1996).
[24] J. M. Ball, P. Cesana, and B. Hambly, MATEC Web Conferences **33**, 02008 (2015).